International Journal of Science and Research (IJSR)
ISSN (Online): 2319-7064
Index Copernicus Value (2013): 6.14 | Impact Factor (2013): 4.438

Optimization of Fracture Behavior of AA6061 Al-Alloy Pipes Using Finite Element Analysis

D.U.M. Manikanta [1], **A. Chennakesava Reddy**[2]

[1]PG Student, Department of Mechanical Engineering, JNTUH College of Engineering, Kukatpally, Hyderabad 500085, India

[2]Professor, Department of Mechanical Engineering, JNTUH College of Engineering, Kukatpally, Hyderabad 500085, India

Abstract: ***In this paper 3D finite element analysis and Taguchi technique were employed to investigate fracture criteria of 6061 Al-alloy pipes subjected to internal bursting pressure. The ultimate tensile strength and yield strength criteria were used to study the failure of pipes. It was observed that the J-integral was proportional to the deformation under the applied bursting pressure. It was noticed that the major dominating control factors which could influence the failure of pipes were the pipe thickness, depth of crack and the bursting pressure.***

Keywords: AA6061, bursting pressure, fracture criteria, crack depth, crack length, J-integral, stress intensity factor, Taguchi technique.

1. Introduction

Metal tubing is used to transfer liquids, air, or solids. Metal tubing is used in heating, ventilation, and air conditioning (HVAC) and plumbing systems and for applications in the aerospace, automotive, chemical processing, food and beverage, manufacturing, and medical industries. AA6061 is used for heavy duty structures requiring good strength-to-weight ratio with good corrosion resistance. The most important parameters in designing pipelines are the pressure and temperature of the conveying media. The major concern of pipes is to maintain its geometric integrity to ensure they are safe and effective during operation to avoid unforeseen disaster. One of the major geometric integrity of the pipe is cracks on its surface. The wall thinning on a pipe due to corrosion, results in localized pit with different depths and lengths on its internal and external surfaces [1], [2]. The codes such as BS 7910 [3] and DNV RP-F101 [4] are the semi-empirical methods used for the assessment of the integrity of pipes. The operating pressure calculation and consequent wall thickness of gas transmission pipelines can be obtained from ASME B31.8 (ASMEB31.8 2012):

$$P = (2\,\sigma t)/D \times F \times E \times \quad (1)$$

where P is the design pressure (MPa), σ is the specified minimum yield strength (MPa), t is the nominal wall thickness (mm), D is the nominal outside diameter (mm), F is the design factor, E is the longitudinal joint factor and T is the temperature derating factor.

As demonstrated in figure 1, analysis of fracture mechanics is described as three pure modes. In mode one (I) or "opening mode" the displacement of crack surfaces due to normal stresses, are perpendicular to the plane of the crack. In forward shear or mode two (II) or "sliding mode", the displacement of crack surfaces is in the plane of the crack and normal to the crack front line. The "tearing mode" or mode three (III) is caused by anti plane shear and the crack surface displacements are parallel to the crack front line and in the plane of the crack. The stress intensity factor (SIF) represented by capital K. The K subscripts I, II and III stands for different loading conditions.

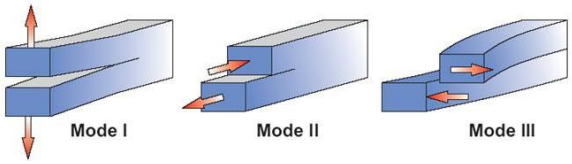


Figure 1: Modes of crack

In a pure elastic crack, stress singularity at the crack tip is dominant. Due to the yield stress of materials especially in metals, for stresses above the σ_y the material deforms plastically. So stress singularity cannot exist. Figure 2 illustrates an approximate stress distribution at the crack tip with a plastic zone. Irwin argues that the crack tip plasticity causes lower stiffness and larger displacements than in the elastic case [5].

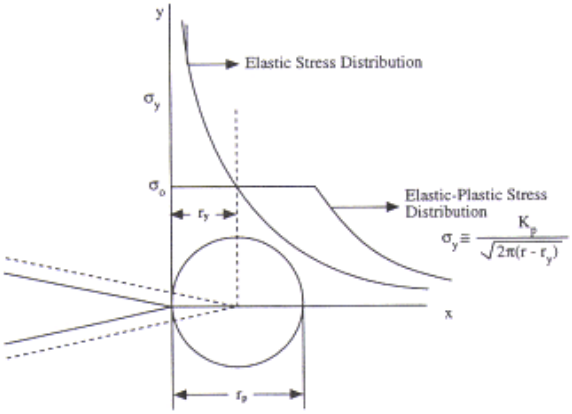


Figure 2: Elastic and Elastic-Plastic crack tip stress distribution in front of the crack tip and the plastic zone sized r_y and r_p

Similar to linear elastic cases, an energy release rate for nonlinear elastic bodies can be defined as the area on the load displacement diagram between crack areas A and $A+dA$, as shown in figure 3. The nonlinear energy release rate J, for constant load and constant displacement has been defined as:

Licensed Under Creative Commons Attribution CC BY

$$J = \left|\frac{\partial \pi}{\partial A}\right| \quad (2)$$

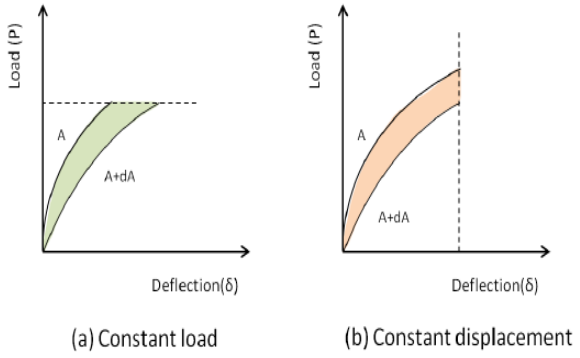


Figure3: Available energy for crack extension in a non linear elastic material under different conditions.

The finite element analysis (FEA) is one of the most efficient tools to quantify reliably the remaining strength of corroded pipes. Elastic-Plastic finite element models have been used to provide more accurate results in evaluating the corrosion defects [6]. ANSYS [7] can be used to numerically evaluate the collapse pressure of crack defects. When a corrosion/flaw defect occurs on the internal or external pipe surface, the integrity of the pipe is reduced. The important parameters that determine the strength of a pipe are as follows [8]:

- Internal pressure
- Pipe Diameter
- Crack depth related to the wall thickness
- Crack length related to the pipe length
- Stress distribution
- Total deformation
- J-integral
- Stress intensity factors (SIFs): KI, KII and KIII

The present work is aimed at to study the finite element analysis of crack propagation and pipe bursting with predefined flaws of varying length and depth. The pipes are analyzed for various bursting pressures. As illustrated in 1igure 1, the longitudinal crack length is shown at 2*a* and the pipe is under an internal pressure loading of *p*, with the pipe thickness depicted as *t*.

2. Materials and Methods

Experiments were performed on 6061 Al alloy pipes. The control parameters are those parameters that a manufacturer can control the design of the product, and the design of process. The levels chosen for the control parameters were in the operational range of 6061 aluminum alloy. Each of the three control parameters was studied at three levels. The chosen control parameters are summarized in table 1. The orthogonal array (OA), L9 was selected for the present work. The control factors were assigned to the various columns of O.A. The assignment of control factors along with the OA matrix is given in table 2.

Table 1: Control factors and their levels

Factor	Symbol	Level–1	Level–2	Level–3
Thickness, mm	A	0.89	1.24	1.47
Length of crack, mm	B	28.2	47.3	60.0
Depth of crack	C	0.56	0.64	0.71
Pressure	D	3.5	4.0	4.5

Table 2: Orthogonal Array (L9) and control factors

Treat No.	A	B	C	D
1	1	1	1	1
2	1	2	2	2
3	1	3	3	3
4	2	1	2	3
5	2	2	3	1
6	2	3	1	2
7	3	1	3	2
8	3	2	1	3
9	3	3	2	1

A surface notch as shown in figure 4 made on the outer surface of the specimen was used as a pre flaw for experimentation. Outer surface notches provide an indication of system response to discontinuities originating from the outer surface. The dimensions of notch are given in figure 4. Outer surface notches were produced in the middle of the tube length by electric discharge machining (EDM).

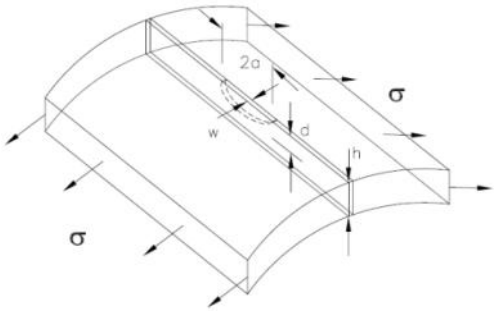


Figure 4: The Crack dimensions.

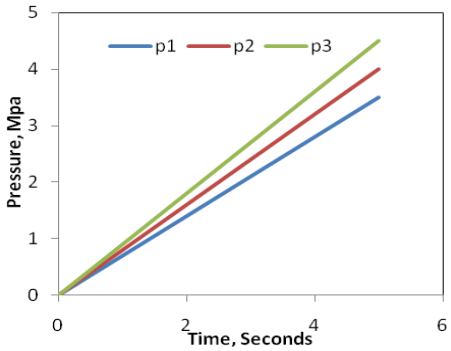


Figure 5: Bursting pressures

The time dependent pressure input was given to burst the pipes. the pressure inputs are given in figure 5. the pressure gradually was increased to avoid sudden burst of pipes. When the pressure was still increased the specimen was burst at the notch.

3. Finite Element Modeling

The cross-section of the pipe was created in 2-D and then it was extruded for the given pipe length along the z-direction [9]. The ANSYS code was used to model the pipe and initial

Licensed Under Creative Commons Attribution CC BY

semi-elliptical crack. The pipe was modeled with tetrahedron elements. The crack and pipe dimensions are given in table-1. The crack geometry is shown in figure 4. Fracture module method for crack generation required that elements be of higher order. Therefore, out of choice of tetrahedral elements of type SOLID 186 were chosen for accurate results [10], [11], [12]. Fine mesh was used to model the crack region. The number of elements and nodes were 1,18,765 and 2,39,558 respectively. A three-dimensional semi-elliptical crack was initiated on the shaft surface. The crack was oriented with respect to pipe axis. In order to create the semi-elliptical crack onto to the surface, a local coordinate system was established. With reference to the local co-ordinate system and the crack was created on the outer surface of the pipe as shown in figure 6. The time dependent pressure was applied on the inner surface of pipe.

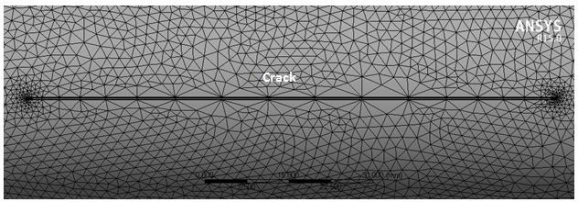


Figure 6: Mesh view of crack on the pipe surface.

Stress intensity is defined as the largest of the absolute values of σ_1 - σ_2, σ_2 - σ_3, or σ_3 - σ_1 [13]:

$$\sigma_I = \text{MAX}\left(|\sigma_1 - \sigma_2|, |\sigma_2 - \sigma_3|, |\sigma_3 - \sigma_1|\right) \quad (3)$$

Stress intensity is related to the maximum shear stress:

$$\sigma_I = 2\tau_{max} \quad (4)$$

Elastic strain intensity is defined as the largest of the absolute values of ε_1 - ε_2, ε_2 - ε_3, or $\varepsilon 3$ - $\varepsilon 1$:

$$\varepsilon_I = \text{MAX}\left(|\varepsilon_1 - \varepsilon_2|, |\varepsilon_2 - \varepsilon_3|, |\varepsilon_3 - \varepsilon_1|\right) \quad (5)$$

Elastic strain intensity is equal to the maximum shear elastic strain:

$$\varepsilon_I = \gamma_{max} \quad (6)$$

The maximum equivalent stress safety tool is based on the maximum equivalent stress failure theory for ductile materials, also referred to as the von Mises-Hencky theory. The discretized form of the J-Integral is given by:

$$J = \sum_{ie=1}^{ne}\left[\sigma_{ij}\frac{\partial u_j}{\partial x_1} - w\,\delta_{1i}\right]\frac{\partial q}{\partial x_i} w_{iw} A_{ie} \quad (7)$$

where n_e is the number of elements to be integrated, w_{iw} is the weight function, and A_{ie} is the area of the element represented by i_e.

For higher-order elements (such as SOLID186), the q vector at mid-side nodes takes the averaged values from the corresponding corner nodes. For a 3-D problem, domain integral representation of the J-Integral becomes a volume integration, which again is evaluated over a group of elements. The implementation becomes more complicated; however, the principal is similar to the 2-D problem. The near-crack-tip behavior of stress is usually thought to be that of plane strain. K_I, K_{II}, K_{III} were obtained from KCALC command.

4. Results and Discussion

The finite element software was carried out twice with two mesh densities according Taguchi design of experimentation.

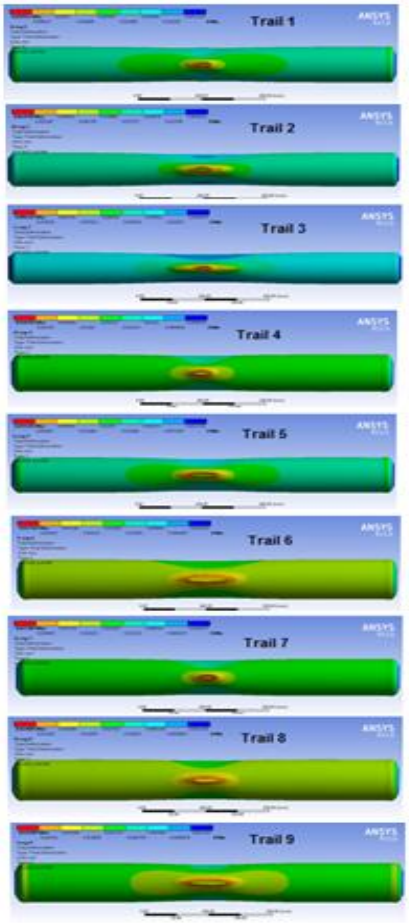


Figure 7: Total deformation of test coupons.

4.1 Static Deformation

Figure 7 gives the total deformation values of tested pipes with different crack geometry and bursting pressure. It was observed that the maximum total deformation of 8.6432×10^{-2} mm with trial no.3 and the minimum total deformation of 2.1084×10^{-2} mm with trail no.9. In both the cases the thickness (1.47 mm) of pipe and crack length (60.0 mm) was same. The crack depths for trial no.3 and trial no.9 were 0.71 mm and 0.64 mm respectively.

4.2 Stress distribution across the crack

Table 3 gives the ANOVA (analysis of variation) summary of equivalent stress. The Fisher's test column establishes all the parameters (A, B, and D) accepted at 90% confidence level. The percent contribution indicates that the thickness parameter, A contributes 70.23% of variation, C (depth of crack) assists 12.75% of variation, and D (pressure) contributes 15.13% of variation on the effective stress. The influence of crack length is negligible.

Licensed Under Creative Commons Attribution CC BY

Table 3: ANOVA summary of the effective stress

Source	Sum 1	Sum 2	Sum 3	*SS*	*v*	*V*	*F*	*P*
A	3730.02	2021.8	1760.22	381475.1	2	190737.5	56782	70.23
B	2486.62	2338.36	2687.06	10208.27	2	5104.135	1519	1.88
C	2108.08	2401.68	3002.28	69250.83	2	34625.42	10307	12.75
D	2096.3	2358.6	3057.14	82220.71	4	20555.18	6119	15.13
Error				23.51	7	3.359086	1.00	0.01
T	10421.02	9120.44	10506.7	543178.4	17			100

Note: *SS* is the sum of square, *v* is the degrees of freedom, *V* is the variance, *F* is the Fisher's ratio, *P* is the percentage of contribution and *T* is the sum squares due to total variation.

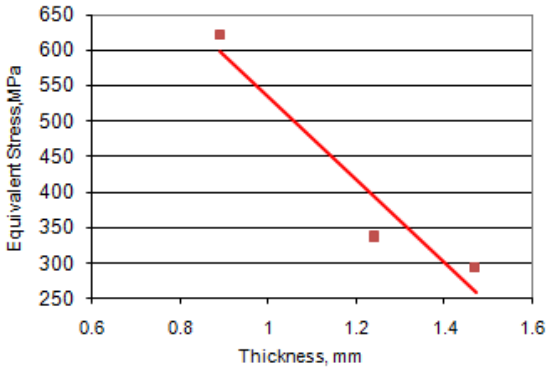


Figure 8: Effect of thickness on the effective stress.

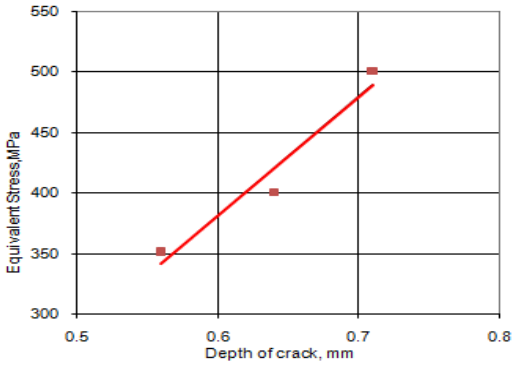


Figure 9: Effect of crack depth on the effective stress.

The equivalent stress decreases with an increase in the thickness of pipe as shown in figure 8. In fact the stress is the force per unit area. As the denominator (i.e. the area) increases, the stress induced in the pipe decreases. The cross-sectional area of the pipe depends on the thickness. As the depth of crack increases the equivalent stress also increases as shown in figure 9. This is due to reduction of the effective cross-sectional area of the pipe. The effective stress induced in the pipe increases with an increase in the bursting pressure as shown in figure 10. The equivalent stress distribution across the crack for all the test coupons is shown in figure 11. The maximum equivalent stress of test coupons 1, 2, 3, 4, 5, 6, 7, 8 and 9 were found to be 485.33 MPa, 551.27 MPa, 826.41 MPa, 408.70 MPa, 323.95 MPa. 275.7 MPa, 348.28 MPa, 290.46 and 237.37 MPa respectively. The equivalent stresses of trials 1, 2, 3, 4, 5 and 7 exceed the ultimate tensile strength (310 MPa) of 6061 aluminum alloy whereas the equivalent stress values of trials 6, 8 and 9 were within the limits of ultimate tensile strength. The equivalent stresses of trials 1, 2, 3, 4, 5, 7 and 8 exceed the yield strength (276 MPa) of 6061 aluminum alloy whereas stress values of trials 6 and 9 were within the limits of yield strength.

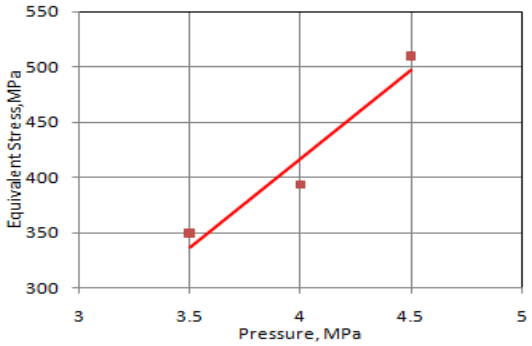


Figure 10: Effect of bursting pressure on the effective stress

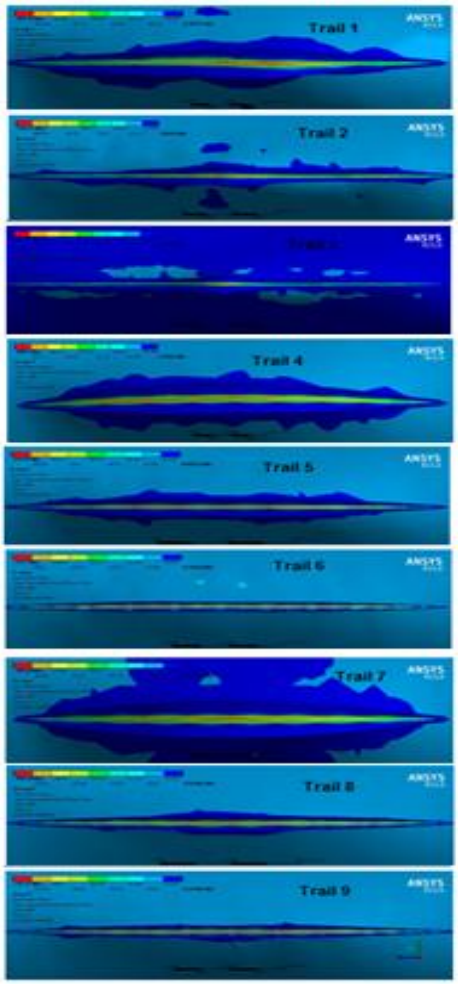


Figure11: Equivalent stress along crack front

4.3 J-integral

The path dependence of the J-integral is displayed for all nine specimens are shown in figure 12. For a crack in an

Licensed Under Creative Commons Attribution CC BY

elastic body subject to a load, the elastic energy stored in the body is a function of two independent variables: the displacement of the load, and the area of the crack. The total displacement of the test coupons 1, 2, 3, 4, 5, 6, 7, 8 and 9 were respectively 0.046mm, 0.062mm, 0.086mm, 0.036mm, 0.032mm, 0.027mm, 0.028mm, 0.025mm and 0.021mm. The maximum value of J-integral was 1.1082 MJ/mm^2 with third trial having the displacement of 0.086mm. The minimum value of J-integral was 0.0879 MJ/mm^2 with ninth trial having the displacement of 0.021mm. Therefore, the J-integral is directly proportional to the displacement of the load applied on the pipe. The path dependence of the J-integral was much more significant in a large deformation analysis [14]. The far field value of J was reached with test coupon 3 latter, whereas in the test coupon 9 having small deformation the far field value of J was already reached. The shear stress values of the test coupon 3and 9 were 417.30 MPa, and 117.83 MPa respectively. The shear strength of AA6061 aluminum alloy was 207 MPa.

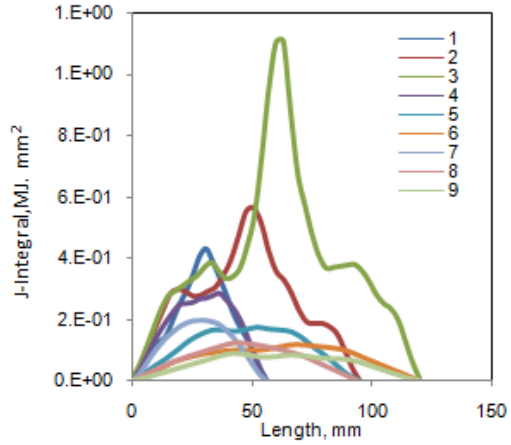


Figure 12: J-Integral values of all trials.

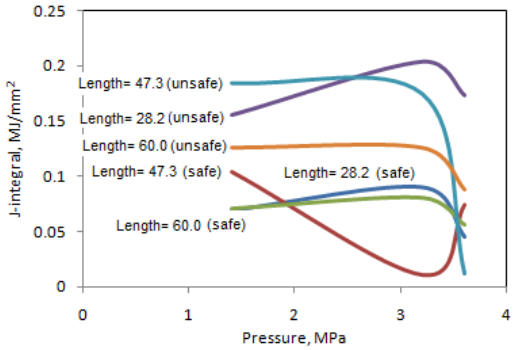


Figure 13: Effect of crack length on the J-integral.

The crack area depends upon the crack length and crack depth. So, the J-integral depends on the crack length and crack depth too. The crack area for the test coupons 1, 2, 3, 4, 5, 6, 7, 8 and 9 were nearly 15.792 mm^2, 30.27 mm^2, 38.4 mm^2, 18.04mm^2, 33.58 mm^2, 33.6 mm^2, 20.02 mm^2, 26.48 mm^2 and 38.4 mm^2 respectively. The effect of crack length and crack depth on the J-integral are shown in figures 13 and 14. It is observed that the effect of crack length is not much influential as compared to the depth of crack on the J-integral. The J-integral is high for the crack depth of 0.64 mm and it is low for the crack depth of 0.71mm. The safe mode is defined as the ratios of equivalent stress to ultimate tensile strength and equivalent stress to yield strength must be less than unity, otherwise it is unsafe mode for the failure analysis of pipes.

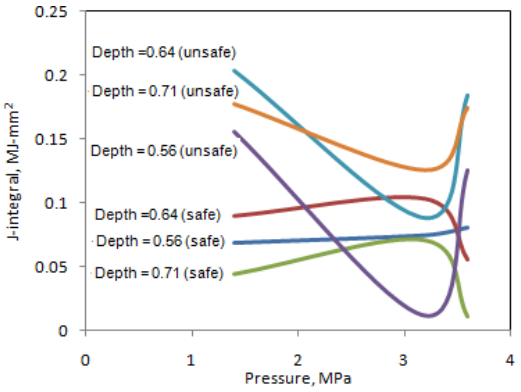


Figure 14: Effect of crack depth on the J-integral.

4.4 Stress intensity factor (KI)

Each test coupon was started with a pre-existing crack of a given length "2*a*". Mode I was a spreading apart of the two halves of the crack interface, recognizable as the most severe case. The stress intensity factor (K) is a defined as the product applied macroscale stress (σ), the square root of the crack length (a), and a constant that depends on the particular fracture mode and geometry of the test specimen. Figure 15 shows the variations of stress intensity factor, KI along the initial crack-front for all pipes. The stress intensity factors, KII and KIII are not discussed here because they are not highly influential factors as compared stress intensity factor KI. The pipe 3 has the maximum value (267.75) of KI whereas the pipe 9 has the minimum value (68.216) of KI.

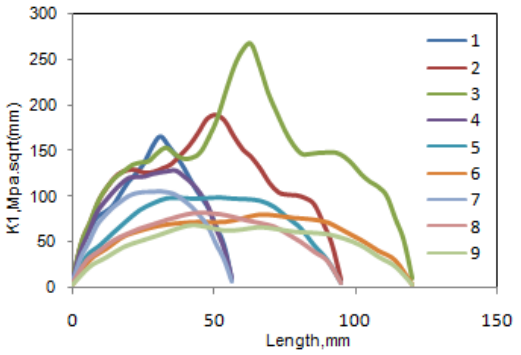


Figure 15: KI values of all trials.

4.5 Failure criteria

If the failure is defined by material yielding, it follows that the design goal is to limit the maximum equivalent stress to be less than the yield strength of the material:

$$\frac{\sigma_e}{S_u} < 1 \quad (8)$$

An alternate but less common definition states that fracturing occurs when the maximum equivalent stress reaches or exceeds the ultimate strength of the material:

$$\frac{\sigma_e}{S_y} < 1 \quad (9)$$

The ANOVA summary of ultimate tensile strength (UTS) and yield strength (YS) failure criterion are given in table 4 and 5. The Fisher's test column ascertains the parameters (A, B,

Licensed Under Creative Commons Attribution CC BY

C and D) accepted at 90% confidence level influencing the variation in the impact strength. The percent contribution indicates that the thickness of the pipe only contributes 69.21% and 66.85% of the variation for UTS and YS criterion respectively, parameter, C (depth of crack) aids 13.36% and 12.87% of variation for UTS and YS criterion respectively, bursting pressure, D gives 14.51% and 16.95 of variation for UTS and YS criterion respectively and the crack length gives negligible contribution.

Table 4: ANOVA summary of the UTS failure criteria

Source	Sum 1	Sum 2	Sum 3	*SS*	*v*	*V*	*F*	*P*
A	11.76	6.37	5.60	3.75	2	1.88	486.78	69.21
B	7.81	7.42	8.49	0.1	2	0.05	12.98	1.71
C	6.63	7.55	9.54	0.73	2	0.37	94.76	13.36
D	6.61	7.48	9.63	0.8	4	0.2	51.92	14.51
Error				0.026	7	0.004	1.00	1.21
T	32.82	28.82	33.27	5.40	17			100

Table 5: ANOVA summary of the YS failure criteria

Source	Sum 1	Sum 2	Sum 3	*SS*	*v*	*V*	*F*	*P*
A	13.02	7.38	6.28	4.35	2	2.175	281.53	66.85
B	9.0722	8.29	9.32	0.1	2	0.05	6.47	1.3
C	7.3999	8.72	10.56	0.85	2	0.425	55.01	12.87
D	7.4544	8.27	10.96	1.13	4	0.282	36.57	16.95
Error				0.054	7	0.007	1.00	2.03
T	36.94	32.68	37.14	6.48	17			100

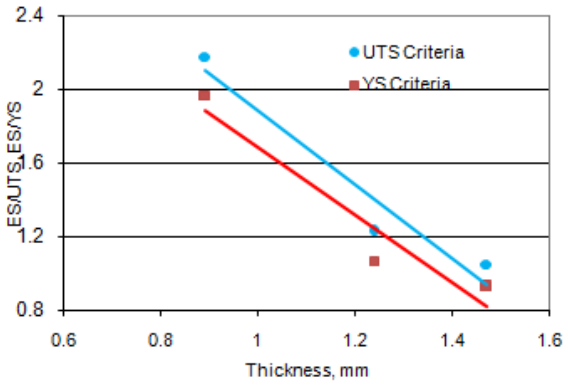


Figure 16: Effect of pipe thickness on failure criterion.

The yield strength and tensile strength of 6061 Al alloy are 276 MPa and 310 MPa respectively. The effect of pipe thickness on the failure criteria is depicted in figure 16. It is noticed that the failure of pipes decreases with an increase in the pipe thickness based on under both the ultimate tensile strength and yield strength criterion. With an increase in the depth of crack and the bursting pressure the failure rate increases. It is also observed that the survival of pipes under ultimate tensile strength criteria is better than the with yield strength criteria. This is owing to fact that the ultimate strength is higher than the yield strength of the material. The failure criteria are plotted for all the test coupons in figure 19. The test coupons 6 and 9 are satisfying both the UTS and YS failure criteria only. Among 6 and 9 the test conditions of test coupon 9 are safer than the test coupon 6.

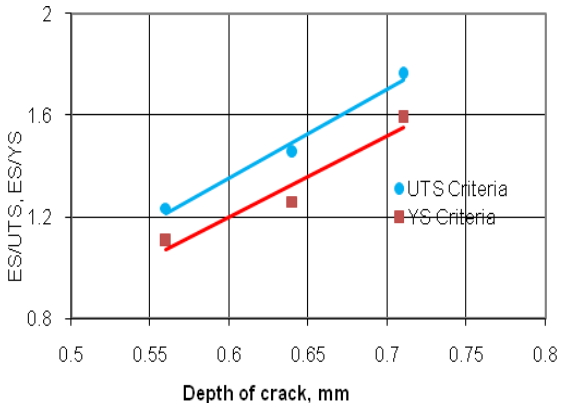


Figure 17: Effect crack depth on the failure criterion.

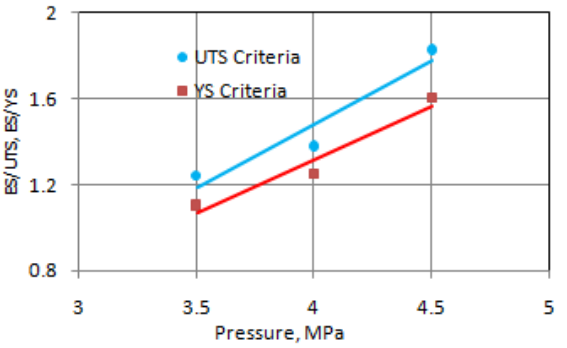


Figure 18: Effect of bursting pressure on the failure criterion.

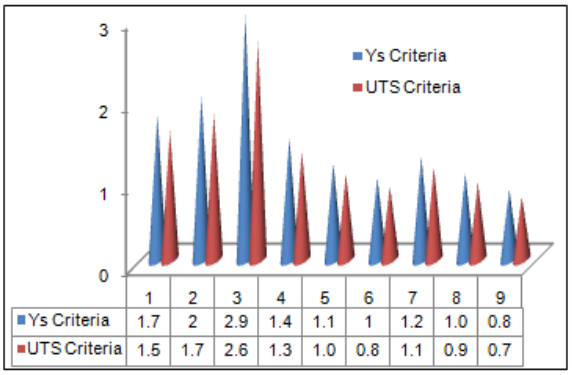


Figure19: Failure criteria based on yield and tensile strengths based on different bursting pressures

5. Conclusions

During crack propagation analysis it was observed that the path dependence of the J-integral was significant during the large deformation of pipes subjected to internal bursting pressure. The predominant control factors of pipe failure were the pipe thickness, depth of crack and bursting pressure. The allowable depth of crack and the bursting pressure were 0.56 mm and 3.5 MPa for the pipe having thickness of 1.24 mm and 0.64 mm and 4.0 MPa for the pipe having thickness of 1.47 mm respectively. The fracture of the pipes was of opening mode (KI).

6. Acknowledgements

The authors thank the University Grants Commission (UGC) – New Delhi for assisting financially this project under PG

Licensed Under Creative Commons Attribution CC BY

project assistantship from SAP-UGC project sanctioned to the Department of Mechanical Engineering, JNT University Hyderabad.

References

[1] P. Hopkins, "Training Engineers in Pipeline Integrity," Western Regional Gas Conference, Arizona, EUA, pp.1-9, 2002.
[2] G. R. K. Kanters,"Pipeline Corrosion and Cracking and the Associated Calibration Considerations for Same Side Sizing Applications," Eclipse Scientific Products Inc., Williamsford, Ontario, Canada.
[3] BS7910, Guide on Methods for Assessing the Acceptability of Flaws in Metallic Structures- Annex G: The Assessment of Corrosion in Pipes and Pressure Vessels, British Standard, 1999.
[4] DNV, Recommended Practice DNV RP-F101 Corroded Pipelines, Det Norske Veritas, Norway, 1999.
[5] G.R.Irwin, "Analysis of stresses and strains near the end of a crack traversing a plate," Applied Mechanics, vol.24, pp.361–364, 1957.
[6] A. Cosham, P. Hopkins,"Best Practice for the Assessment of Defects in Pipelines-Corrosion", Engineering Failure Analysis, pp.1245-1265, 2007.
[7] ANSYS, Inc., www.ansys.com, July 2010.
[8] D. R. Stephens, B. N. Leis, and D. L. Rudland, "Influence of Mechanical Properties and Irregular Geometry on Pipeline Corrosion Defect Behavior", 1997.
[9] Chennakesava R Alavala, "CAD/CAM: Concepts and Applications," PHI Learning Pvt. Ltd., 2008.
[10] Chennakesava R Alavala, "Finite Element Methods: Basic Concepts and Applications," PHI Learning Pvt. Ltd., 2008.
[11] N. Jyothirmayi, A. Chennakesava Reddy, B. Balu Naik, "Finite element analysis of Ti-alloy fracture behavior and experimental validation," National Conference on Advances in Mechanical Engineering, Hyderabad, pp.50-55, 13-14th May, 2005.
[12] A. Chennakesava Reddy, "Finite element analysis of reverse superplastic blow forming of Ti-Al-4V alloy for optimized control of thickness variation using ABAQUS," Journal of Manufacturing Engineering, vol.1(1), pp.6-9, 2006.
[13] Jr. J.Newman, and I. S. Raju, "'An Empirical Stress-Intensity Factor Equation for the Surface Crack," Engineering Fracture Mechanics vol.15, no.1-2, pp.185–192, 1981.
[14] A. Chennakesava Reddy, P. Ram Reddy, B. Kotiveerachari, "Large rotation and large deformation analysis of four-bar mechanism," National Level Technical Symposium Nalgonda, 12th March 2005.

Licensed Under Creative Commons Attribution CC BY